

Stealthy Voice Eavesdropping with Acoustic Metamaterials: Unraveling a New Privacy Threat

Zhiyuan Ning, Zhanyong Tang, Juan He, Weizhi Meng, Yuntian Chen

Abstract—We present SUPEREAR, a novel privacy threat based on acoustic metamaterials. Unlike previous research, SUPEREAR can surreptitiously track and eavesdrop on the phone calls of a moving outdoor target from a safe distance. To design this attack, SUPEREAR overcomes the challenges faced by traditional acoustic metamaterials, including low low-frequency gain and audio distortion during reconstruction. It successfully magnifies the speech signal by approximately 20 times, allowing the sound to be captured from the earpiece of the target phone. In addition, SUPEREAR optimizes the trade-off between the number and size of acoustic metamaterials, improving the portability and concealability of the interceptor while ensuring effective interception performance. This makes it highly suitable for outdoor tracking and eavesdropping scenarios. Through extensive experimentation, we have evaluated SUPEREAR and our results show that it can achieve an eavesdropping accuracy of over 80% within a range of 4.5 meters in the aforementioned scenario, thus validating its great potential in real-world applications.

Index Terms—Privacy Threat, Voice Eavesdropping, Acoustic Metamaterials.

I. INTRODUCTION

PRIVACY spying has become an increasingly severe security threat, with attackers often acquiring sensitive information through various means, typically without the target’s awareness [1]–[7]. Acoustic eavesdropping, as one such method, captures conversations to extract critical information, leading to many risks like account privacy breaches, financial loss, and identity theft [8]–[11]. For example, an attacker might eavesdrop on a target’s private conversations with important clients while they are moving outdoors, using the information to forge transactions or obtain account details.

Existing acoustic eavesdropping attacks can be implemented through various means. In addition to the common method of directly using microphones for eavesdropping, other side-channel eavesdropping methods are typically categorized into methods based on motion sensors [9], [10], [12], [13], optical sensors [14], [15], and radio frequency (RF) sensors [11], [16]. For motion sensor-based acoustic eavesdropping, devices utilize internal accelerometers or similar sensors to capture minute vibrations caused by sound waves. These vibrations can be decoded into voice signals even if the device does not directly record audio. Optical sensor-based acoustic eavesdropping involves monitoring minute vibrations on surfaces such as light bulbs or windows. Using optical sensors to detect physical changes induced by sound waves, attackers can

reconstruct conversations in a room. RF sensor-based acoustic eavesdropping analyzes the impact of sound waves on the propagation of RF signals to reconstruct voice information. In the aforementioned eavesdropping attacks, motion sensor-based acoustic eavesdropping requires intrusion into the target device. Compared to other types of eavesdropping attacks, this method increases the risk of detection and exposure.

Motivations. Research [9], [11], [17], [18] reveals that eavesdropping on a target’s phone call during travel is a common phenomenon, as depicted in Fig. 1. Human auditory perception features selective attention, meaning that in complex environments, individuals usually concentrate on expected sounds, such as the voice of the other caller, while ignoring the potential risk of eavesdropping. However, existing eavesdropping methods in the above-mentioned scenario have two drawbacks. First, the sound output from the phone’s earpiece during calls is significantly lower than that of the speaker. This privacy-related feature results in the signal-to-noise ratio (SNR) dropping below the detection limit of traditional eavesdropping methods when the distance exceeds 2 meters [1]. Secondly, previous non-invasive eavesdropping methods rely on precisely targeting the medium vibrating with the target sound (e.g., a phone’s back). However, in outdoor tracking scenarios, the constant movement of both the medium and the eavesdropping device makes accurate targeting challenging.

The development of acoustic metamaterial technology [19]–[28] has brought possibilities for addressing the drawbacks of traditional attack methods. By manipulating the interference of sound signals within its internal structure, acoustic metamaterials can significantly enhance the SNR of earpiece signals [29], effectively overcoming the limitations of traditional eavesdropping methods in low SNR environments. Additionally, acoustic metamaterials can directly capture sound signals widely propagated in the air, enabling eavesdropping from any position within a certain radius of the target without the need for precise aiming [30], [31].

Although the use of metamaterials for eavesdropping offers certain advantages, several challenges arise when implementing a complete system. One challenge is that traditional acoustic metamaterials enhance low-frequency ranges by complicating their internal structures. However, this design significantly increases thermo-viscous losses, leading to a substantial reduction in gain [32], which in turn weakens eavesdropping performance. Another issue is that while a multi-metamaterial system can improve coverage of speech frequency bands and eavesdropping performance by increasing the number of metamaterials, it also compromises the system’s portability, making it difficult to achieve an optimal

Zhiyuan Ning, Zhanyong Tang, Juan He and Yuntian Chen are with the School of Information Science and Technology, Northwest University, Xi’an, China (e-mail: zytang@nwu.edu.cn). Weizhi Meng is with the School of Computing and Communications, Lancaster University, United Kingdom. (e-mail: w.meng3@lancaster.ac.uk)

balance between performance and concealment. Additionally, the gain curve of acoustic metamaterials may introduce audio distortion, particularly in the form of manufacturing-related gain jumps and uneven gain distribution across frequencies. Furthermore, these materials simultaneously amplify both the audio signal and noise, resulting in environmental noise that significantly degrades the reconstructed audio quality.

Contributions. To address the above challenges, SUPEREAR introduces some key improvements: ① A novel method for constructing a multi-metamaterial system has discovered how to enhance low-frequency gain by adjusting structural parameters, rather than traditionally increasing the internal structure of the metamaterials, thus avoiding thermo-viscous losses; ② Optimization of the enhanced frequency range and determine the minimum number of metamaterials required within this range, to improve system portability without compromising eavesdropping performance, making it ideal for mobile scenarios; ③ Use of a smoothing filter algorithm to eliminate frequency jump points and an adaptive gain adjustment algorithm to counteract audio distortion caused by gain imbalances. Leveraging the frequency selectivity of the multi-metamaterial system effectively suppresses ambient noise interference in the reconstructed audio, significantly reducing audio distortion and enabling SUPEREAR to efficiently and accurately intercept target phone calls while moving.

We demonstrate that SUPEREAR can be implemented using low-cost, off-the-shelf commercial components, such as the Raspberry Pi, microphone arrays, and resin 3D-printed acoustic metamaterials. Due to the passive nature of the metamaterials, SUPEREAR requires no additional power source, ensuring portability and long-duration eavesdropping capability. Additionally, it can directly capture high-quality audio signals without relying on machine learning models. We comprehensively evaluated SUPEREAR under various conditions, and experimental results show excellent performance, effectively tracking and eavesdropping on phone calls from a distance of 4.5 meters, posing a new privacy threat.

The main contributions of this paper are as follows:

- We propose a portable and covert eavesdropping system, named SUPEREAR, based on acoustic metamaterials, and open-sourced the relevant code¹. This system is designed to eavesdrop on the target's phone calls during travel, without requiring intrusion into the target device or reliance on machine learning, posing a new privacy threat.
- We address three key challenges in using acoustic metamaterials for eavesdropping and successfully extend SUPEREAR's eavesdropping range to 4.5 meters.
- We demonstrate how to build an efficient eavesdropping system using low-cost 3D printing technology and evaluate SUPEREAR's performance through experiments under different devices and environmental interferences.

The rest of the paper is organized as follows. Sec. II begins by introducing the background and related work on acoustic eavesdropping and acoustic metamaterials. Building on this foundation, Sec. III provides an overview of our approach. Next, Sec. IV delves into the challenges we encountered and



Fig. 1. A potential attack scenario involves the traveling target making a private phone call in a public space while the attacker uses SUPEREAR to eavesdrop from 4.5 meters.



Fig. 2. Voice output during calls vs. voice output in other situations

the corresponding solutions. Sec. V then describes the system's components and implementation in detail. Following that, Sec. VI presents the experiments conducted and analyzes the results. Sec. VII extends the discussion to potential directions for improving our work. Subsequently, Sec. VIII explores possible defense measures against our system. Finally, Sec. IX concludes the paper.

II. BACKGROUND AND RELATED WORK

A. Acoustic Eavesdropping Attacks

Eavesdropping attacks on voice communications have been widely proven to pose significant privacy and security risks. Previous research on eavesdropping attacks has covered various techniques, including RF (Radio Frequency) sensing [1], [11], [16], [33]–[39], motion sensor-based sensing [8]–[10], [12], [15], [40]–[44], and optical sensing [14], [45], [46]. These techniques each have distinct characteristics and are suited to different application scenarios.

In the field of RF sensor-based acoustic eavesdropping, research using millimeter waves has become relatively mature. This technology captures minute vibrations on objects using high-frequency millimeter waves and reconstructs the sound signals from them [1], [11], [16]. Additionally, motion sensor-based acoustic eavesdropping utilizes sensors like accelerometers and gyroscopes to capture tiny vibrations caused by sound waves [8]–[10], [15], [40], [42], [43]. Optical sensor-based acoustic eavesdropping detects vibrations on the surface of objects caused by sound waves, enabling long-distance data collection without physical contact with the target device [14], [45].

However, RF sensor-based eavesdropping [1], [11], [16], [33]–[38], [47] and optical sensor-based eavesdropping [14], [45], [46] typically rely on fixed or limited-range observable media, but in outdoor mobile environments, maintaining continuous and precise tracking of the medium becomes challenging, thereby limiting the practical application of these techniques. On the other hand, motion sensor-based eavesdropping [8]–[10], [12], [13], [40]–[43] are susceptible to the additional interference from target movement and environmental noise-induced vibrations in dynamic outdoor settings, making it difficult to effectively separate target audio from interference. Furthermore, these methods require intrusion into the target device, significantly increasing the attacker's risk of exposure.

B. Acoustic Metamaterials

In recent years, acoustic metamaterials have gained widespread attention for their compact design and excep-

¹The code is available at: <https://github.com/helo0507/SuperEar>

tional performance in sound wave control. Some of these metamaterials can effectively enhance or focus sound waves within specific frequency ranges, while their passive nature provides the advantage of low power consumption, demonstrating broad application potential across various fields. For example, in acoustic imaging, metamaterials can precisely control the propagation direction and focus of sound waves, improving the resolution of ultrasound imaging, and are widely used in medical imaging and non-destructive testing [48]–[50]. In sound localization and enhancement, metamaterials can optimize sound propagation in specific directions at a lower cost, improving the clarity and localization accuracy of audio systems, with applications in headphones, speakers, and conference systems [51], [52]. Additionally, acoustic metamaterials show great potential in the application of soundproof barriers. By absorbing surrounding sound wave energy and concentrating it within, metamaterials can significantly reduce the sound energy in the external area, achieving efficient noise isolation in fields such as buildings and transportation [32], [53], [54].

Due to these unique properties, acoustic metamaterials exhibit potential for acoustic eavesdropping in mobile environments. However, their narrow frequency enhancement range and uneven gain distribution can result in distortion during audio reconstruction. Additionally, these materials amplify both target audio signals and environmental noise, making it more challenging to effectively suppress noise interference in outdoor settings.

C. Challenge in eavesdropping on voice output during calls

As shown in Fig. 2, in non-private information-sharing scenarios, phones typically use speakers to play audio, dispersing voice over open spaces beyond 10 meters. In contrast, during private calls, users bring their ears close to the phone (within 5 cm), and the phone’s earpiece employs beamforming technology to protect privacy, directing most of the voice energy precisely to the user’s ear while minimizing voice leakage into the air [11]. Consequently, the voice transmission distance of the earpiece in the air is significantly shorter than that of the speaker, with the signal-to-noise ratio (SNR) generally falling below the detection threshold beyond 2 meters [1], [11]. Furthermore, in outdoor tracking scenarios, complex environmental factors further reduce the voice transmission distance of the earpiece, making it even more challenging to eavesdrop on target phone calls in such settings.

D. Motivations

Most existing eavesdropping research struggle to achieve effective eavesdropping on phone calls (see [8]–[10], [14]–[16], [34], [36], [38], [40], [42], [45], [46]) or eavesdropping on the phone calls, but only allows the target to move within the precise targeting range of non-portable eavesdropping devices (see [1], [11]). However, these assumptions are not always applicable. In many real-world scenarios, the target may be making a phone call while moving in public spaces, forcing the attacker to carry eavesdropping equipment to track and eavesdrop in real-time, which significantly increases the

difficulty of implementing traditional eavesdropping assumptions. The unique properties of acoustic metamaterials [29], [30], [32] inspire us to design a miniaturized, highly concealed attack system that can accurately eavesdrop on the target’s phone calls from a safe distance outdoors, addressing many common application scenarios.

E. Threat Model

In this threat model, the victim is targeted while in motion. The attacker employs a portable and miniaturized eavesdropping system to eavesdrop from a *safe distance*, defined as the distance at which the target does not notice the attacker. As per related research [55]–[57], a distance greater than 3 meters is considered a public distance that does not draw the attention of strangers. Additionally, the attack setting does not require complete soundproofing and allows for normal ambient noise, enabling the attacker to operate in most cases.

III. OVERVIEW OF OUR APPROACH

Our SUPEREAR consists of a Raspberry Pi terminal, eight compact passive acoustic metamaterials, and a microphone array embedded within the metamaterials. Detailed system configuration is provided in Sec. V. As shown in Fig. 3 and Algorithm 1, the eavesdropping attack is divided into multiple steps, described in detail below.

Capture Audio Signals. In the initial stage of the attack, SUPEREAR captures the target’s phone call audio signal group *V1*, providing high-quality raw data for subsequent processing (line 10).

Process Audio Signals. Since each metamaterial enhances only a specific frequency range, and the audio signal may be affected by noise and distortion, further processing is required.

- 1) Combine voice signals: Extract and recombine the enhanced audio to generate the complete target audio signal *V2* (see Section IV-B) (line 13).
- 2) Reduce noise: First, real-time monitoring of background noise *N* is performed to assess interference (line 9). Subsequently, the SUPEREAR’s *Noise Suppression Algorithm* (see Section IV-C) is used to isolate noise frequency bands, and *SoX* [58] is applied to eliminate residual noise and interference (line 14).
- 3) Remove jumps and balance gain: Apply the *Distortion Suppression Algorithm* (see Section IV-C) to eliminate jump points and use dynamic gain adjustment to reduce distortion, ensuring the output audio *V4* remains high-fidelity (line 15).

IV. SYSTEM DESIGN FOR SUPEREAR

To accurately eavesdrop on the phone calls of moving targets at a safe distance using acoustic metamaterials, we need to address the following challenges:

Challenge 1. How can we enhance low-frequency performance of acoustic metamaterials without causing high thermo-viscous losses and reducing the gain?

Challenge 2. The design of a multi-metamaterial system significantly affects its portability and concealability. Therefore,

Algorithm 1: The framework of our approach

```

1 Activate Raspberry Pi
  // Start the eavesdropping attack.
2 Activate Audacity
3 attackOverview()
4 Function attackOverview():
5   Step1()
6   Step2(N, VI)
7   return Step2(N, VI)
8 Function Step1():
9   // Capturing voice signals
10  Receive environmental noise signal N.
11  // Use SUPEREAR and microphone array.
12  Receive enhanced audio signals VI.
13  return N, VI
14 Function Step2(N, VI):
15  // Processing voice signals
16  // Use Spectrum Reassembly Algorithm.
17  Crop and recombine VI to obtain V2.
18  // Use SUPEREAR and SoX for noise reduction.
19  Denoise V2 using the noise signal N to obtain V3.
20  // Use Distortion Suppression Algorithm.
21  Remove distortion from V3 to obtain V4.
22  // V4 is enhanced high-quality audio signal
23  return V4
  
```

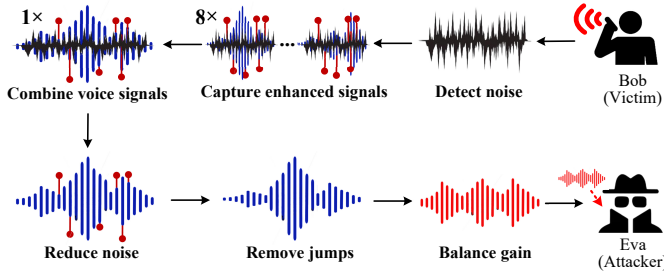


Fig. 3. SUPEREAR’s Voice Privacy Spy Flow (After capturing and enhancing the audio, we reorganize the enhanced frequencies while performing noise reduction and distortion minimization.)

the selection and sizing of acoustic metamaterials are crucial considerations. How can we determine the optimal number and dimensions of these acoustic metamaterial components?

Challenge 3. How can we eliminate the distortion caused by defects in acoustic metamaterials during audio reconstruction and suppress the negative impact of noise on the reconstructed audio?

A. Solution to Challenge 1: Construct a new multi-metamaterial system with high gain in the low-frequency range

We first examine how acoustic metamaterials utilize the coiling-up space structure of Mie resonators to enhance sound pressure and further analyze the limitations of existing studies in adjusting the low-frequency signal enhancement capabilities of metamaterials.

The basic structure of the acoustic metamaterial is shown in Fig. 4a, featuring a curved propagation path with a path width of $a = 3.2$ mm, wall thickness of $t = 0.8$ mm, outer diameter of $D = 80$ mm, inner diameter of $d = 14$ mm, and a channel with $N = 8$ turns. When sound waves enter the path from any

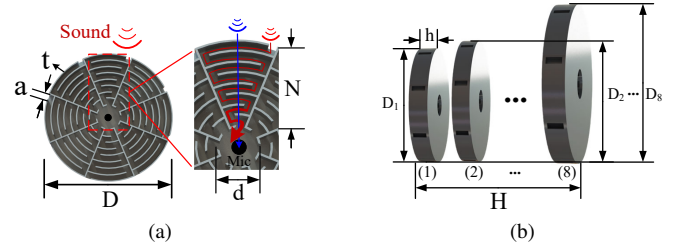


Fig. 4. (a) Structure of acoustic metamaterials. we place the microphone at the center of the structure. (b) The system of acoustic metamaterials.

direction, the sound pressure output at the central microphone can be expressed using the following equation:

$$P = P_0 \cdot \frac{n_r}{\lambda_0} \cdot \sqrt{\frac{2\rho c^2}{\lambda_0^2}} \quad (1)$$

where P_0 is the input sound pressure, n_r is the refractive index, λ_0 is the wavelength of the sound wave in air, ρ is the density of the medium, and c is the speed of sound.

As shown in Eq. 1, to enhance the outgoing sound pressure P around the microphone, it is essential to increase the refractive index n_r . Hence, the acoustic metamaterial achieves sound pressure amplification by increasing n_r . Specifically, the refractive index n_r can be approximated as the ratio of the length of the red path to the length of the blue straight path in Fig. 4a. When sound waves propagate through a curved path with a high refractive index n_r , their energy becomes significantly concentrated at the microphone location, resulting in a sound pressure increase of about 16 times. Additionally, the amplification effect of acoustic metamaterials depends on their resonant frequency. The resonant frequency is determined by the geometric parameters of the metamaterial structure, including the number of channels N and its dimensions. For the aforementioned acoustic metamaterial, the resonant frequency is 563 Hz, with an enhancement range of approximately 100 Hz, allowing it to effectively amplify sound signals within a specific frequency range.

To enable the aforementioned metamaterial to function effectively in the low-frequency range, prior research [32] proposed increasing the number of internal channels N within the metamaterial to reduce its resonant frequency. For instance, when $N = 22$, the resonant frequency of the metamaterial can be reduced to approximately 260 Hz.

However, increasing N significantly exacerbates thermo-viscous losses during sound wave propagation within the metamaterial. Specifically, as N increases, the sound wave’s propagation path becomes more curved and complex, resulting in more reflections, refractions, and scattering within the channels. This not only increases friction and resistance between the sound waves and the medium but also extends the propagation time, causing more energy to dissipate as heat and leading to higher thermo-viscous losses. As a result, the maximum gain multiplier in the 250 Hz to 300 Hz range is limited to just 5 times [32], significantly reducing the effectiveness of eavesdropping. To address this issue, we propose the following innovative approach:

Enhancing the gain of metamaterials in the low-frequency range. To address the aforementioned challenge, we develop

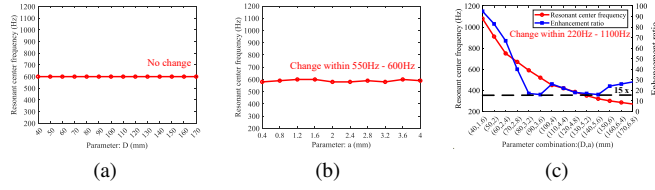


Fig. 5. (a) The result of changing parameter D . (b) The result of changing parameter a . (c) The result of simultaneously changing parameters D and a .

a new multi-metamaterial system design method. Specifically, instead of increasing the number of internal channels N in the metamaterial, we focus on exploring the relationship between other key parameters of the metamaterial and its resonant frequency.

Based on this, we conducted an in-depth analysis of the metamaterial structure shown in Fig. 4a, with a particular emphasis on two key parameters: diameter D and path width a . By varying D and a while keeping the channel number N constant, we explored their relationship with the resonant frequency in COMSOL, and the results are shown in Fig. 5.

As shown in Fig. 5a and Fig. 5b, variations in the geometric parameter D do not alter the central frequency within the frequency enhancement range of the metamaterial, while changes in the geometric parameter a only cause slight shifts in the central frequency within a 50 Hz range. Neither variation curve meets our requirements for low-frequency enhancement.

When we adjust both D and a simultaneously, as shown in Fig. 5c, the central frequency undergoes significant changes. To more efficiently determine the resonant central frequency f_c corresponding to different parameter combinations, we summarize their relationship in the following equation:

$$f_c = k \times f_{c,0} \times \frac{(D_0, a_0)}{(D, a)} \quad (2)$$

where, $f_{c,0} = 563\text{Hz}$ represents the initial resonance center frequency, while $D_0 = 80\text{mm}$ and $a_0 = 3.2\text{mm}$ are the initial metamaterial parameters. To determine the proportionality factor k , we need to conduct an in-depth analysis of the curve shown in Fig. 5c. Firstly, it can be observed that as the geometric parameters D and a increase proportionally, the resonance center frequency of the metamaterial gradually decreases. Secondly, it is important to note that the effect of D and a on f_c is not linear; as D and a continue to increase, the rate of decrease in f_c gradually slows down. Based on the above analysis, We can divide k into four stages for discussion based on the value of D . Therefore, the resonance center frequency of the multi-metamaterial system can be expressed as:

$$f_c = \begin{cases} 1.89 \times f_{c,0} \times \frac{(D_0, a_0)}{(D, a)}, & \text{when } 40 \leq D < 60, \\ 1.25 \times f_{c,0} \times \frac{(D_0, a_0)}{(D, a)}, & \text{when } 60 \leq D < 100, \\ 0.99 \times f_{c,0} \times \frac{(D_0, a_0)}{(D, a)}, & \text{when } 100 \leq D < 140, \\ 0.87 \times f_{c,0} \times \frac{(D_0, a_0)}{(D, a)}, & \text{when } 140 \leq D \leq 170. \end{cases} \quad (3)$$

The derivation of Eq.3 enables us to use different combinations of metamaterial parameters to construct a multi-metamaterial system for voice enhancement.

Subsequently, we verified the gain of the metamaterials with different parameter combinations using COMSOL. As shown in Fig. 5c, the new multi-metamaterial system can achieve a maximum gain of over 15 times in the low-frequency range. This demonstrates that our design effectively avoids high thermo-viscous losses, significantly improving the gain performance.

B. Solution to Challenge 2: Determine the optimal gain range and amount of metamaterials

Determine the optimal gain range. To achieve the optimal metamaterial design, it is essential to first define the key frequency range for speech enhancement. Although the speech frequency range spans from 250 Hz to 4000 Hz, studies have shown that humans can clearly understand speech when the audio frequency band is close to 1000 Hz [47], [59]. This is because the recognition of vowels is crucial for speech comprehension, and nearly all the first formants (F1 formant) of vowels fall within the range of 250 Hz to 1000 Hz. Therefore, we have set the frequency enhancement range for speech to be between 250 Hz and 1000 Hz.

Determine the optimal amount of metamaterials. After defining the frequency enhancement range, we needed to design a metamaterial system to match this range. According to the relationship between metamaterial parameters and resonant center frequency in Eq. 3, we observed that in the narrower range of 250 Hz to 550 Hz, the resonant frequency of metamaterials changes relatively slowly, and their bandwidth is also narrower, averaging about 87.5 Hz. Therefore, 4 metamaterials are required to fully cover this frequency range. In the range of 550 Hz to 1000 Hz, the resonant frequency of metamaterials changes more quickly, and the bandwidth is broader, averaging about 157.5 Hz. Consequently, 4 metamaterials are also needed to cover this range. Specifically, SUPEREAR consists of eight metamaterials, as shown in Fig. 4b, the diameters of these eight metamaterials (1) - (8) are $D_1 = 50\text{ mm}$, $D_2 = 60\text{ mm}$, $D_3 = 70\text{ mm}$, $D_4 = 80\text{ mm}$, $D_5 = 100\text{ mm}$, $D_6 = 120\text{ mm}$, $D_7 = 140\text{ mm}$, and $D_8 = 160\text{ mm}$, with a thickness of $h = 15\text{ mm}$ for each metamaterial. Therefore, the total thickness when stacked together is $H = 120\text{ mm}$. As shown in Fig. 6a, this combination of acoustic metamaterials effectively covers the frequency range (250 Hz to 1000 Hz) while maintaining the overall compactness of the device.

Spectrum crop and stitch. Since the eight audio signals from the metamaterial system only exhibit enhancement effects within specific frequency ranges, we need to trim each frequency range further and merge them into a single, continuous audio signal to achieve broad frequency coverage. As shown in Fig. 6b, we trimmed the spectrum to remove the overlapping portions due to the overlap in the enhancement frequency ranges of each metamaterial, maximizing enhancement efficiency and avoiding redundancy. Specifically, we conducted a detailed analysis of the frequency response of each metamaterial, identifying the frequency point with the highest gain within the overlapping regions and using it as the basis for trimming. For the eight metamaterials, we trimmed at 320 Hz,

TABLE I
PARAMETER COMBINATIONS OF ACOUSTIC METAMATERIALS.

| label | path width (a) | Diameters (D) | Frequency range |
|-------|--------------------|-------------------|------------------|
| (1) | 2 mm | 50 mm | 820 Hz - 1000 Hz |
| (2) | 2.4 mm | 60 mm | 720 Hz - 880 Hz |
| (3) | 2.8 mm | 70 mm | 580 Hz - 730 Hz |
| (4) | 3.2 mm | 80 mm | 520 Hz - 660 Hz |
| (5) | 4 mm | 100 mm | 430 Hz - 550 Hz |
| (6) | 4.8 mm | 120 mm | 350 Hz - 440 Hz |
| (7) | 5.6 mm | 140 mm | 290 Hz - 360 Hz |
| (8) | 6.4 mm | 160 mm | 250 Hz - 320 Hz |

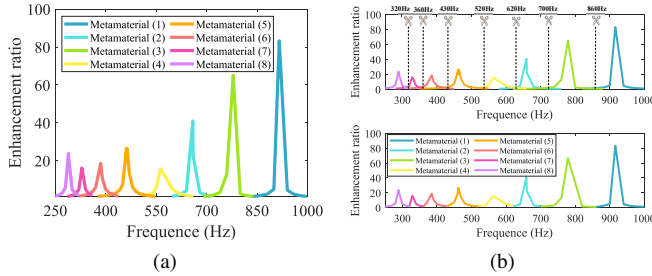


Fig. 6. (a) Enhancement curve of metamaterial systems. (b) Spectrum cropping for metamaterial system.

360 Hz, 430 Hz, 520 Hz, 620 Hz, 700 Hz, and 860 Hz to remove overlapping areas and ineffective edge bands, ensuring that only the most effective frequency range with the highest gain of each metamaterial is retained.

After completing the spectrum trimming, we stitched together the enhanced frequency ranges of the eight metamaterials, achieving continuous and broad coverage of the voice frequency range. To verify whether the metamaterial quantity and frequency range selection were optimized, we conducted further validation in subsequent experiments (see details in Sec VI-C3).

C. Solution to Challenge 3: Reduce distortion and suppress noise.

Although the improved SUPEREAR with the optimal design can enhance a wide range of speech frequencies, it may still lead to distortion in the audio signal. There are three main issues: (1) As shown in Fig. 7, specific frequencies within the enhancement range of the metamaterials exhibit a jump in enhancement, with gains exceeding 1500 times. This situation can distort the audio signal and affect the accuracy of eavesdropping. We speculate that this may be due to manufacturing defects during the 3D printing process of the metamaterials, leading to uneven material distribution in their internal structure or outer walls, thus affecting the gain multiplier; (2) Observing the enhancement curves in Fig. 6a, it is evident that the gain multipliers of the metamaterials vary across different frequencies, primarily due to differences in their resonant frequencies. This inconsistency results in uneven audio quality, significantly impacting the effectiveness of eavesdropping. (3) The metamaterials struggle to distinguish between noise and audio signals at the same frequency, leading to simultaneous amplification. Under the interference of environmental noise, the eavesdropping effectiveness of SUPEREAR is significantly

impacted. We implemented the following measures to address *Challenge 3*.

Eliminate jump points. To address the frequency jump problem, we implemented a smoothing algorithm based on median filtering and threshold replacement to reduce abrupt changes in frequency response. Specifically, we first evaluated the gain jump points in the metamaterial enhancement curve by calculating the gain difference $\Delta G(f_i) = |G(f_i) - G_{\text{median}}(f_{i-1}, f_i, f_{i+1})|$, where G_{median} represents the median of the current frequency and its neighboring frequencies. If the gain difference $\Delta G(f_i)$ exceeds the defined threshold (mean plus three times the standard deviation, as simulation results show that the gain difference between adjacent frequencies does not exceed this value), the point is identified as a jump point. For each jump point, we replace its gain with the median of its neighboring frequencies, which can be expressed as: $G_{\text{new}}(f_i) = G_{\text{median}}(f_{i-1}, f_i, f_{i+1})$. We continued processing the remaining gain curve and repeated the process until no more jump points were found. The gain curve after smoothing is shown in Fig. 7. Through this method, we effectively removed the jump points, significantly improved the smoothness of the gain curve, and enhanced the stability of the audio signal, ultimately achieving a more accurate and coherent target audio.

Maintain frequency gain balance. To address the issue of gain mismatch among the metamaterials, we employed an adaptive gain adjustment algorithm. This algorithm dynamically adjusts the gain based on real-time feedback from different frequency bands, ensuring balance among the gains of the various metamaterials while maintaining the overall enhancement effectiveness of the system as much as possible. Specifically, the core of adaptive gain adjustment lies in reducing the gain coefficient for frequency bands with higher gain through $G_{\text{new}} = \frac{G_{\text{target}}}{G_{\text{actual}}}$ to avoid excessive enhancement. For frequency bands with lower gain, the gain coefficient is increased by $G_{\text{new}} = \frac{G_{\text{actual}}}{G_{\text{target}}}$ to reach the target gain G_{target} . The target gain G_{target} is determined by calculating the median of the gain curve, which effectively eliminates the influence of extreme values and more accurately reflects the overall gain distribution. This median-based adaptive adjustment can effectively balance the gain across different frequency bands, reducing imbalances and significantly optimizing the overall quality of the audio signal.

We collectively refer to the methods for eliminating jumps and balancing gains as the *Distortion Suppression Algorithm*. After processing with the *Distortion Suppression Algorithm*, the final gain curve is shown in Fig. 8. Unlike in Fig. 6a, where high gain is achieved only at specific frequencies, the gains of various metamaterials now tend to be consistent within the 250 Hz to 1000 Hz, all around 20 times, effectively reducing audio signal distortion.

Suppress noise interference. Acoustic metamaterials enhance audio signals and amplify the noise within their effective range, making deploying SUPEREAR in noisy environments more challenging. To address this, we propose a frequency-selective noise suppression method to mitigate the interference of environmental noise on SUPEREAR. Specifically, the enhanced

Algorithm 2: Noise Suppression Algorithm

```

1 Noise Suppression()
2 Function Noise Suppression():
3   Step1()
4   Step2(f0)
5   return Step2(f0)
6 Function Step1():
7   // Detect noise frequency range
8   Receive noise and analyze frequency range f0.
9   return f0
10 Function Step2(f0):
11   // Suppress noise gain.
12   for i = 1 to 8 do
13     // fi are the ranges enhanced by metamaterials.
14     if fi contains f0 then
15       fi ← Isolate from the combined range
16     end
17   end
18   Combine the remaining fi into a new spectrum F
19   return F

```

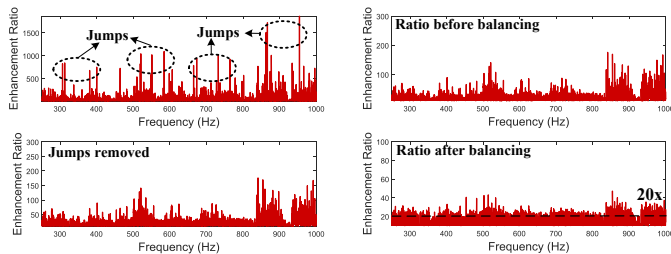


Fig. 7. Remove jumps in the enhancement curve

Fig. 8. New enhancement curve after balancing.

frequency range of SUPEREAR is formed by combining eight independent metamaterials. This design allows us to effectively isolate the metamaterials within the noise frequency band during the spectrum composition process, thereby minimizing the impact of noise on the overall audio quality. This method is called the *Noise Suppression Algorithm*.

To validate the feasibility of this algorithm, we first conducted research and field studies to gather data on various types of outdoor noise and their frequency ranges. Specifically, natural environmental noise (such as wind and rain) is primarily concentrated between 20 Hz to 300 Hz [60], [61], while urban traffic noise (such as sounds from car engines and wheels) typically falls within the 50 Hz to 500 Hz range [62], [63]. This indicates that outdoor noise is generally concentrated in the low-frequency range, only slightly overlapping with the enhanced frequency range of SUPEREAR, thereby confirming the feasibility of the *Noise Suppression Algorithm*.

Based on the feasibility validation above, we implemented the *Noise Suppression Algorithm*, as shown in Algorithm 2. When noise within the enhanced frequency range of the metamaterials is detected during eavesdropping, SUPEREAR automatically suppresses the gain of the corresponding metamaterial, significantly reducing noise interference. Although this method may impact the quality of the reconstructed audio, we validated through experiments that these impacts are completely acceptable compared to the interference caused by noise (see details in Sec. VI-D2).

TABLE II

THE TEST OBJECTS INCLUDE FIVE TYPES OF MOBILE DEVICES AND OS VERSIONS OF NINE MODELS. DIFFERENT VOLUNTEERS ARE ALSO SELECTED.

| Targets type | Model/Name | OS/Gender |
|--------------|-----------------|-----------------|
| Apple | iPhone 14 Pro | IOS 17.4.1 |
| | iPhone 13 | IOS 17.2.1 |
| | iPhone 12 | IOS 16.5.1 |
| Samsung | Galaxy S7 | Android 8.0.0 |
| | Pixel 3 | Android 12.0.0 |
| Google | Pixel 2 | Android 10.0.0 |
| Xiaomi | Redmi K50 Ultra | Miui 13.0.10 |
| | Mi10 Lite Zoom | Miui 12.0.6 |
| Huawei | nova 7 SE 5G | HarmonyOS 3.0.0 |
| Volunteers | Mary | Female |
| | John | Male |
| | Jack | Male |

V. IMPLEMENTATION

The SUPEREAR prototype consists of 8 acoustic metamaterial modules made from resin (manufactured through 3D printing), a low-cost commercial microphone array (model MSM261S4030HOR digital silicon microphone), and a Raspberry Pi 5b. The Raspberry Pi 5b is a high-performance, compact computer capable of efficiently handling the tasks of SUPEREAR while ensuring the portability of the system. As shown in Fig. 9a, when the microphone array captures the audio signals enhanced by the metamaterials, the signals are transmitted to the Raspberry Pi 5b for further processing. The Raspberry Pi 5b serves as the control terminal of the system, responsible for correcting distortion caused by the metamaterials, suppressing noise, and seamlessly integrating audio from different enhanced frequency ranges to reconstruct the final audio.

As shown in Fig. 9b, after assembly, SUPEREAR can be easily placed into a handbag measuring approximately 27 cm in length and 16 cm in width, making it highly portable. The device’s portability allows it to be widely applicable in various mobile attack scenarios.

VI. EVALUATION

A. Experimental Setup and Methodology

Test targets. We evaluated the eavesdropping performance of SUPEREAR on five mainstream smartphone brands, including Apple [64], Samsung [65], Google [66], Xiaomi [67], and Huawei [68]. In our evaluation, nine devices were used, and their specifications are listed in Table II. In addition, to test SUPEREAR’s eavesdropping capability on the voices of persons during calls (not voices of the microphone), we invited three volunteers (one female and two males) to participate in the experiments.

Metrics. Table III lists the quantified metrics used in our evaluation.

Success Rate of eavesdropping is an essential criterion for assessing the reliability of SUPEREAR. In each experiment, we conducted 30 eavesdropping tests on each target device or volunteer. If the Mel-Cepstral Distortion (MCD) value of the reconstructed audio from the attack is below 8, the attack is considered successful [16], [69]. MCD represents the difference in Mel-Frequency Cepstral Coefficients (MFCC)

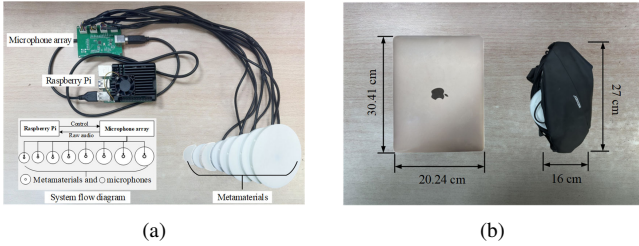


Fig. 9. Implementation of SUPEREAR: (a) The prototype of SUPEREAR, (b) The covert prototype of SUPEREAR (smaller in size than a MacBook Air 13-inch).

TABLE III
EVALUATING METRICS

| Metrics | Description |
|---------------|--|
| Success Rate | Success Rate is the ratio of successful attacks (MCD value below 8) to the total number of attacks (30 attacks in each experiment) [16], [69]. |
| RSA | RSA is the <i>Range</i> at which SUPEREAR can <i>Successfully Attack</i> (with a success rate of over 80%) [9]. |
| Word Accuracy | Word Accuracy is the ratio of the number of correctly recognized words in audio to all words [9], [11], [13]. |
| MOS | Mean opinion score (MOS) is a subjective evaluation metric that assesses the intelligibility of reconstructed audio based on human judgments. [8], [71]. |

characteristics between the reconstructed and original audio. A smaller MCD value indicates a higher similarity, reflecting better audio reconstruction quality.

RSA is used to evaluate the eavesdropping range of SUPEREAR. We determine the RSA by checking whether SUPEREAR can achieve a success rate of 80% or higher within the specified range.

Word Accuracy is measured using Google Text-to-Speech AI (TTS) [70] technology, which assesses the proportion of correctly recognized reconstructed audio.

Mean Opinion Score (MOS) is a subjective evaluation metric based on human understanding of the reconstructed audio. To assess this, we recruited ten volunteers, equally divided by gender. To avoid bias, these volunteers participated in the experiment voluntarily and received no compensation. Participants first listened to the reconstructed audio, followed by the original audio. They were then asked to rate the similarity between the reconstructed and original audio on a scale from 1 to 5 (with higher scores indicating more remarkable similarity).

Experiment Design. We conducted a series of experiments to simulate real phone call scenarios: positioning the earpiece of the target device close to the ear to play the phrase *My bank card password is "1234567890"*. with the earpiece output set to an average conversation volume of around 60 dB. Subsequently, the target volunteer repeated the phrase, keeping the volume at approximately 45 dB, which is a whisper-level volume.

The details of each experiment are shown in Table IV. Firstly, experiments A1 to A4 were conducted to test the eavesdropping effectiveness of SUPEREAR on different target devices and human voices. Secondly, experiments B1 to B3



Fig. 10. Real attack scenarios: (a) C1: Eavesdropping attacks against walking targets (the target's speed is 2 m/s and 3 m/s), (b) C2: Eavesdropping attacks against environmental noise (60 dB - 70 dB).

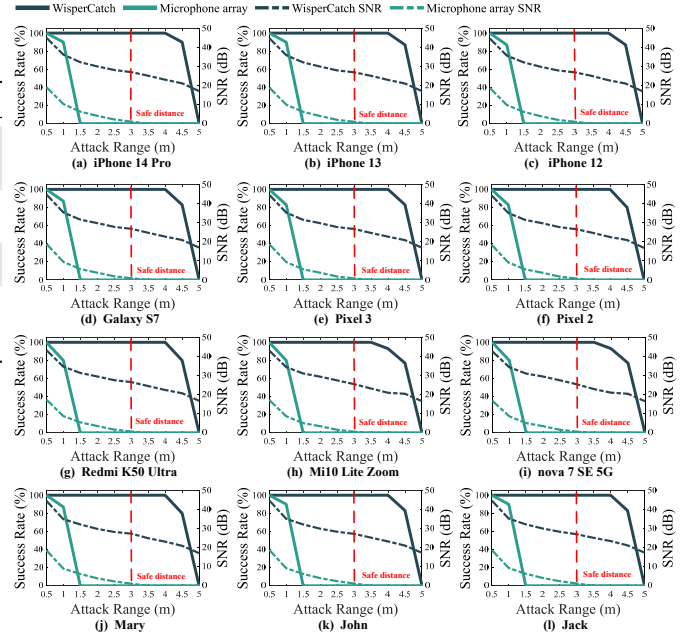


Fig. 11. Performance of SUPEREAR and microphone array on various targets

were designed to evaluate the enhancements brought by the innovations of SUPEREAR. Both experiments, A1 to A4 and B1 to B4 were conducted in a laboratory environment with a background noise level of approximately 43 dB. Additionally, experiments C1 and C2 assessed the attack performance of SUPEREAR in real-world scenarios, including noise environments and attacks on moving targets. As shown in Fig. 10, the suitable attack distances for experiments C1 and C2 exceeded 4 meters, during which the SNR of the audio emitted by the phone's earpiece fell well below the detection limit. We believe these scenarios are shared in real life, but prior eavesdropping research struggles to adapt to them fully. Finally, we compared SUPEREAR with prior research on eavesdropping attacks to highlight its advantages in experiment D.

Our experiments were approved and overseen by the University's IRB (Institutional Review Board) to ensure compliance with data security measures and ethical guidelines for data processing.

B. Eavesdropping performance of SUPEREAR

1) A1 - *The real enhancement effect of SUPEREAR* : To ensure accurate long-distance eavesdropping, SUPEREAR must effectively amplify audio within a specific voice frequency

TABLE IV
LIST OF EXPERIMENTAL SETTING

| Test objectives | Label | Test focus | Description |
|---------------------------------------|----------------|---|--|
| Eavesdropping performance of SUPEREAR | A1 (Sec.VI-B1) | The real enhancement effect of SUPEREAR | To validate the real performance of the SUPEREAR design, we examined its sound enhancement effect in the real world. |
| | A2 (Sec.VI-B2) | Eavesdropping range for different targets | To test the impact of range and different targets to SUPEREAR, we let SUPEREAR attack the various devices or people (mentioned in Table II) at different ranges. |
| | A3 (Sec.VI-B3) | Eavesdropping performance of human subjective auditory evaluation | To assess the subjective audibility of the SUPEREAR, we invited volunteers to evaluate the similarity between the reconstructed audio and the original audio. |
| | A4 (Sec.VI-B4) | Eavesdropping accuracy against passwords | To test the eavesdropping accuracy of SUPEREAR, we had the target send a voice message saying, "The password is 123456780," and then measured how far SUPEREAR could accurately eavesdrop. |
| Enhancement capability of SUPEREAR | B1 (Sec.VI-C1) | Capability of SUPEREAR's multi-metamaterial system | To test the advantages of SUPEREAR's multi-metamaterial combined system, we compared its performance with that of a single metamaterial. |
| | B2 (Sec.VI-C2) | Capability of SUPEREAR's <i>Distortion Suppression Algorithm</i> | To test SUPEREAR's ability to handle distortions caused by the metamaterials, we compared the performance between SUPEREAR and the system with unprocessed distortions. |
| | B3 (Sec.VI-C3) | Capability of SUPEREAR's optimal metamaterial design | To test whether the metamaterials chosen for SUPEREAR are the most portable and effective, we compared the performance between SUPEREAR and other combinations of metamaterials. |
| Performance in real world scenarios | C1 (Sec.VI-D1) | Eavesdropping attacks against walking targets | To test SUPEREAR's performance in attacking against walking targets, we attacked a target who is moving on the street, and the target's speed is 2 m/s and 3 m/s (as shown in Fig. 10a). |
| | C2 (Sec.VI-D2) | Eavesdropping attacks in noise environment | To evaluate SUPEREAR's performance in overcoming noisy environments, we tested SUPEREAR in two typical noise settings: natural ambient noise and traffic noise (as shown in Fig. 10b). |
| Compared to prior research | D (Sec. VI-E) | Advantages of SUPEREAR in tracking and eavesdropping on phone calls | To verify whether SUPEREAR can achieve more covert and user-friendly eavesdropping attacks, we compared it with prior attack systems. |

range. Using the audio sample *My bank card password is "1234567890"*, we measured SUPEREAR's enhancement performance in the 250 Hz - 1000 Hz range. As shown in Fig. 12, the experimental results indicate that SUPEREAR can achieve approximately 20 times enhancement within the target frequency range.

2) *A2 - Eavesdropping range for different targets*: The eavesdropping range is a crucial factor determining the success or failure of eavesdropping attacks in practical applications, especially when targeting phone calls, where the subjects tend to be more alert. Therefore, a more extensive attack range helps enhance the attacker's concealment. Additionally, individual differences and device characteristics can also affect the performance of SUPEREAR when eavesdropping on different people or electronic devices, as variations exist in vocal cords, vocal tracts, speaking habits, and the performance of different devices' speakers. Therefore, we tested SUPEREAR's maximum attack range on various devices and multiple volunteers, providing the SNR of the reconstructed audio at different distances (specific information about the targets can be found in Table II), with the experimental results shown in Fig. 11.

The experimental results show that SUPEREAR performed exceptionally well on the Apple iPhone 14 Pro, achieving a maximum eavesdropping range of 4.7 meters (success rate over 80%). At this range, the SNR of the reconstructed audio was still maintained at 21.2 dB, likely due to the iPhone's excellent earpiece noise reduction algorithm. In addition, SUPEREAR also performed strongly on other devices, with an average maximum eavesdropping range of 4.5 meters (success rate over 80%) and an average SNR of 20.8 dB for the reconstructed audio. In tests with volunteers, the average maximum eavesdropping distance reached 4.6 meters (success rate over 80%), with an average SNR of 21 dB for the reconstructed audio. This indicates that the differences between devices and indi-

viduals have a minimal impact on SUPEREAR's eavesdropping range, and SUPEREAR can effectively eavesdrop from a *safe distance* across different devices. Notably, the average maximum eavesdropping range of traditional microphone arrays is only 1.3 meters, which is far below the *safe distance* and makes them easy to detect.

SUPEREAR's ability to eavesdrop at a *safe distance* is attributed to its proposed acoustic metamaterial system, which significantly enhances the audio SNR. Compared to traditional microphone arrays, experimental results demonstrate that SUPEREAR performs exceptionally well in tests with various devices and multiple volunteers.

3) *A3 - Eavesdropping performance of human subjective auditory evaluation*: We incorporated human subjective assessments of the reconstructed audio to comprehensively evaluate the eavesdropping performance of SUPEREAR. This subjective assessment can reflect the target's emotional reaction during the conversation. If SUPEREAR can accurately recover the target's tone and emotions, the attacker will better understand the target's intentions.

As shown in Fig. 13, we collected the average MOS from 10 volunteers for reconstructed audio targeting different subjects. The results indicate that the average MOS from all 10 volunteers for each target's reconstructed audio was above 4, signifying that, despite slight distortion, the reconstructed audio maintained a high level of similarity to the original. These findings demonstrate that SUPEREAR excels at preserving the tone and emotional nuances of the target.

4) *A4 - Eavesdropping accuracy against passwords*: Eavesdropping on passwords is a common but hazardous method of information theft. We assume the attacker can steal a victim's financial assets or business secrets by obtaining sensitive and confidential information. The attacker remotely eavesdrops on the target making a phone call and captures when the target

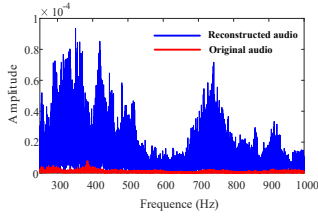


Fig. 12. The real enhancement effect of SUPEREAR

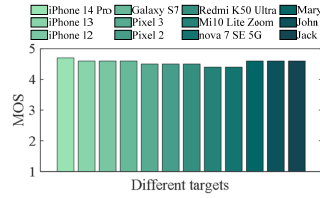


Fig. 13. Performance of human subjective auditory evaluation

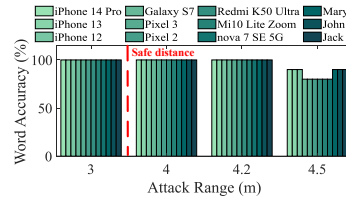


Fig. 14. Eavesdropping accuracy against passwords

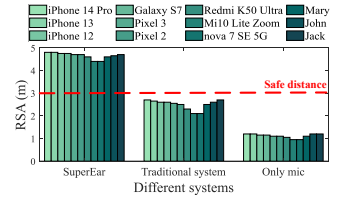


Fig. 15. Capability of SUPEREAR's multi-metamaterial system

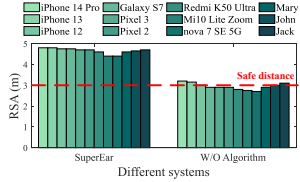


Fig. 16. Capability of SUPEREAR's Distortion Suppression Algorithm

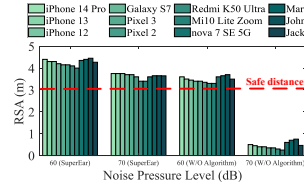


Fig. 17. Impact of noise on SUPEREAR

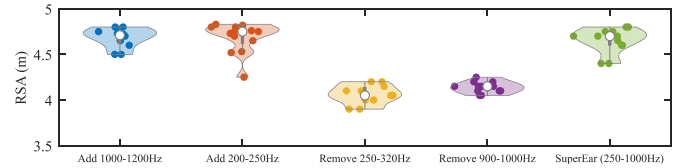


Fig. 18. Capability of SUPEREAR's optimal metamaterial design

quietly discloses their password (*My bank card password is "1234567890"*).

The key to successfully carrying out such eavesdropping attacks is ensuring that the reconstructed audio can accurately reproduce each password digit, which demands high precision from SUPEREAR. Therefore, we tested SUPEREAR's ability to capture and identify characters accurately, focusing on its eavesdropping accuracy at different distances. As shown in Fig. 14, the experimental results indicate that SUPEREAR achieved a 100% word accuracy for all targets at a distance of 4.2 meters, demonstrating its high precision in password eavesdropping.

5) *Summary*: To sum up, the experimental results of A1 to A4 demonstrated that SUPEREAR can conduct high-accuracy eavesdropping attacks on various devices or targets from a *safe distance* while accurately reconstructing the target's emotional expression. Subsequently, in order to verify the effectiveness of the innovations in SUPEREAR, we conducted experiments B1 to B3 as follows.

C. Enhanced Capability of SUPEREAR

1) *B1 - Capability of SUPEREAR's multi-metamaterial system*: The new multi-metamaterial system design of SUPEREAR plays a crucial role in achieving precise long-range eavesdropping. To verify the superiority of SUPEREAR, we conducted ablation experiments comparing its performance with traditional multi-metamaterial systems and microphones in eavesdropping scenarios. Specifically, we evaluated the maximum eavesdropping distance for each system on 12 targets. As shown in Fig. 15, the experimental results indicate that SUPEREAR significantly enhanced the eavesdropping distance, achieving an average RSA of 4.5 meters, which is 86% greater than the traditional system. While the traditional system also showed a significant improvement over the microphone, its average RSA still did not exceed the safe distance, making it more vulnerable to exposure. These data strongly demonstrate the critical role and necessity of SUPEREAR's new multi-metamaterial system design in eavesdropping attacks.

2) *B2 - Capability of SUPEREAR's Distortion Suppression Algorithm*: The *Distortion Suppression Algorithm* of SUPEREAR effectively reduces the distortions caused by manufacturing defects in the metamaterials and the imbalance in gains among multiple metamaterials, thereby significantly enhancing the quality of the audio signals. To verify the superiority of this algorithm, we compared the RSA between SUPEREAR and a metamaterial system without the *Distortion Suppression Algorithm*. As shown in Fig. 16, the experimental results indicate that the RSA of the metamaterial system without the *Distortion Suppression Algorithm* is only 2.94 meters. At the same time, SUPEREAR achieves an improvement of 53%. This also demonstrates that SUPEREAR can only perform eavesdropping at a safe distance with the aid of the *Distortion Suppression Algorithm*, highlighting the necessity of this algorithm.

3) *B3 - Capability of SUPEREAR's optimal metamaterial design*: To adapt to outdoor mobile eavesdropping scenarios, the optimal metamaterial design of SUPEREAR enhances audio quality and emphasizes portability. To verify the superiority of this design, we compared the RSA of SUPEREAR with that of other metamaterial designs. These different designs include: (1) adding one extra metamaterial to enhance audio in the 1000 Hz - 1200 Hz range; (2) adding one extra metamaterial to enhance audio in the 200 Hz - 250 Hz range; (3) removing one metamaterial to omit enhancement in the 900 Hz - 1000 Hz range; (4) removing one metamaterial to omit enhancement in the 250 Hz - 320 Hz range. As shown in Fig. 18, the experimental results indicate that the RSA of designs (1) and (2) is nearly identical to that of SUPEREAR, with only increases of 0.65% and 1.5%, respectively. In contrast, the RSA of designs (3) and (4) decreases by 12.3% and 14.5%, indicating significant performance loss. This further validates that the optimal metamaterial design of SUPEREAR balances exceptional performance and portability.

4) *Summary*: The experimental results indicated that the optimal multi-metamaterial system and distortion suppression algorithm in SUPEREAR complement each other, significantly

enhancing the eavesdropping range while ensuring optimal portability. Next, to verify SUPEREAR’s effectiveness in real attack scenarios with various interferences, we further conducted the following experiments C1 and C2 to evaluate its performance comprehensively.

D. Performance in real-world scenarios

1) *C1 - Attacks against walking victims:* Due to its strong portability and robustness, SUPEREAR is highly suitable for conducting covert eavesdropping on moving targets in outdoor environments. In the scenario shown in Fig. 10a, we invited volunteers carrying different devices to perform tests to evaluate the attack performance at various walking speeds. The volunteers walked at approximately 2 m/s and 3 m/s, representing standard and fast walking, respectively.

The experimental results shown in Fig. 19 indicate that when the target walks at speeds of 2 m/s and 3 m/s and is 4.5 meters away from SUPEREAR, the average attack success rates are 83% and 81.25%, respectively. These results show that SUPEREAR performs equally well when eavesdropping on moving targets, with its RSA remaining stable at 4.5 meters, similar to eavesdropping on stationary targets. Therefore, under normal walking conditions, SUPEREAR can conduct trailing attacks at a safe distance without alerting the target, significantly increasing the likelihood of a successful attack.

2) *C2 - Noise Impact:* The intensity of ambient noise is one of the key factors affecting the success rate of eavesdropping attacks. To verify the effectiveness of SUPEREAR’s *Noise Suppression Algorithm*, we tested its RSA under various noise conditions, maintaining the target’s movement speed at 3 m/s (as shown in Fig. 10b), with the experimental results shown in Fig. 17.

In a noise environment with a frequency range of 20 Hz - 300 Hz and a volume of approximately 60 dB (equivalent to outdoor wind and rain sounds), the average RSA of SUPEREAR remains at 4.26 meters. In contrast, the average RSA of the system without the *Noise Suppression Algorithm* drops to 3.5 meters, showing a significantly higher performance loss. When the noise level rises to 50 Hz - 500 Hz at approximately 70 dB (comparable to traffic noise in urban streets), the average RSA of SUPEREAR decreases to 3.64 meters. We speculate that this is because the noise frequency range is broad and covers some of the critical frequencies of the human voice, which affects the performance of SUPEREAR. However, despite the interference caused by the noise on the signal, the average RSA of SUPEREAR remains within the *safe distance*. In contrast, the average RSA of the system without the algorithm is only 0.46 meters. These results suggest that SUPEREAR can resist environmental noise and successfully execute eavesdropping attacks.

3) *Summary:* The experimental results from scenarios C1 and C2 demonstrate that SUPEREAR can effectively carry out covert eavesdropping attacks across various practical scenarios (e.g., under walking and noise environments).

E. Performance Compared to Prior Research

We compared SUPEREAR with recent acoustic eavesdropping research to verify its applicability for non-intrusive outdoor

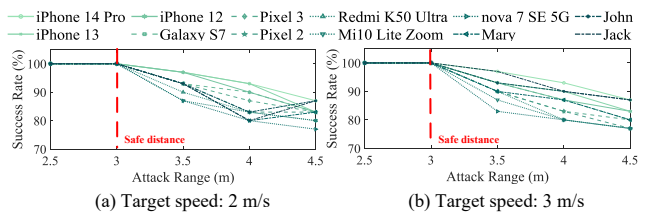


Fig. 19. The impact of moving target’s speeds (target’s speeds are 2 m/s and 3 m/s)

TABLE V
PERFORMANCE COMPARED TO PRIOR RESEARCH

| Name | Earpiece Attack | Non-intrusive | Long range | No aiming |
|-----------------|-----------------|---------------|------------|------------|
| mmEve [1] | Yes | Yes | Yes | No |
| mmSpy [11] | Yes | Yes | No | No |
| mmEcho [16] | No | Yes | No | No |
| EarSpy [44] | Yes | No | Yes | Yes |
| AccelEve [9] | No | No | Yes | Yes |
| Vibphone [13] | Yes | No | Yes | Yes |
| LidarPhone [46] | No | No | Yes | No |
| Lamphone [14] | No | Yes | Yes | No |
| SuperEar | Yes | Yes | Yes | Yes |

tracking eavesdropping of target phone calls.

As shown in Table V, among recent eavesdropping methods, only mmSpy [11], mmEve [1], EarSpy [44], and Vibphone [13] can achieve eavesdropping on earpieces. EarSpy and Vibphone require prior intrusion into the target device, making their application conditions restrictive and inconsistent with our threat model. While mmSpy and mmEve allow non-intrusive eavesdropping, mmSpy’s range is limited to within 2 meters, which may easily alert the target; mmEve performs better for earpiece eavesdropping with a range of 6 to 8 meters, at a *safe distance*, but requires continuous aiming of the millimeter-wave radar at the target device, which is challenging in outdoor tracking scenarios. In contrast, SUPEREAR does not require intrusion into the target device or aiming at the target device, allowing it to handle various complex interferences in mobile tracking eavesdropping, demonstrating a clear advantage.

VII. DISCUSSION

Improvements in Acoustic Metamaterials. Optimizing acoustic metamaterials is essential for enhancing the performance of the SUPEREAR system. Future research can focus on advancing material design to achieve superior enhancement effects. Additionally, to adapt to more complex application scenarios, the size of acoustic metamaterials should be further reduced to improve system concealment. These improvements will significantly increase the practical value of SUPEREAR.

Improvement of Noise Reduction Technology. Although SUPEREAR has effectively suppressed the impact of noise, in certain complex environments, noise can still cause some performance loss. With the continuous advancement of noise reduction technologies, we expect SUPEREAR to integrate with more advanced and efficient noise reduction algorithms, reducing signal distortion caused by noise interference. This will further enhance the system’s robustness and the accuracy of audio reconstruction. Through these technological improvements, SUPEREAR will be able to maintain high-quality

signal capture and audio restoration capabilities, even in more challenging environments, ensuring further enhancement of eavesdropping performance.

VIII. COUNTERMEASURES

Prior defense strategies. Soundproofing materials are an effective defense against acoustic eavesdropping. High-density fiberboards and sound-absorbing foams can block or absorb sound waves [72], [73], reducing their propagation and limiting acoustic eavesdropping ability to capture audible frequencies. Additionally, continuously playing loud white noise can mask sensitive audio, preventing acoustic eavesdropping from extracting valuable information. This approach does not rely on physical barriers but instead disrupts sound wave transmission through interference.

Challenges and future directions in defending against SUPEREAR. Defense strategies based on soundproofing materials have limitations, primarily due to their high cost and lack of flexibility in deployment, making them more suitable for fixed indoor environments. Their application in outdoor or open spaces remains challenging. Sound interference-based defenses, such as using white noise, can mask sensitive audio, but they also significantly increase environmental noise. In outdoor settings, continuous white noise could disturb the public environment. Therefore, both of these defense strategies face challenges when applied to defend against SUPEREAR in outdoor environments. We believe that future research should focus on developing more portable protective devices that can be easily installed on the earpieces of smart devices. These devices would use directional sound transmission to direct the audio directly into the target's ear, preventing sound leakage and effectively countering the threats posed by SUPEREAR.

IX. CONCLUSION

This paper introduced a novel eavesdropping attack system based on acoustic metamaterials called SUPEREAR. By integrating compact, passive acoustic metamaterials, SUPEREAR significantly enhances the performance, portability, and concealment of eavesdropping devices, enabling them to effectively eavesdrop on outdoor mobile targets' phone calls at a *safe distance*. Compared with prior research, our proposed system achieved three key innovations: First, a novel multi-metamaterial system was constructed to extend the enhancement frequency range of the metamaterial while maintaining high gain. Second, an optimized metamaterial design method was proposed, which enhances portability while ensuring system performance. Finally, it successfully eliminated frequency jumps and gain imbalance caused by the metamaterial's own limitations, and suppressed noise interference, further improving eavesdropping effectiveness. In several comparative experiments, SUPEREAR demonstrated outstanding performance in complex and dynamic outdoor environments, significantly outperforming existing technologies in call eavesdropping and related scenarios.

REFERENCES

- [1] C. Wang, F. Lin, T. Liu, K. Zheng, Z. Wang, Z. Li, M.-C. Huang, W. Xu, and K. Ren, "mmve: eavesdropping on smartphone's earpiece via cots mmwave device," in *Proceedings of the 28th Annual International Conference on Mobile Computing And Networking*, 2022, pp. 338–351.
- [2] J. H. Anajemba, C. Iwendi, I. Razzak, J. A. Ansero, and I. M. Okpalaoaguchi, "A counter-eavesdropping technique for optimized privacy of wireless industrial iot communications," *IEEE Transactions on Industrial Informatics*, vol. 18, no. 9, pp. 6445–6454, 2022.
- [3] S. Zhang, Y. Liu, and M. Gowda, "I spy you: Eavesdropping continuous speech on smartphones via motion sensors," *Proceedings of the ACM on Interactive, Mobile, Wearable and Ubiquitous Technologies*, vol. 6, no. 4, pp. 1–31, 2023.
- [4] T. M. Hoang, T. Q. Duong, H. D. Tuan, S. Lambotharan, and L. Hanzo, "Physical layer security: Detection of active eavesdropping attacks by support vector machines," *IEEE Access*, vol. 9, pp. 31 595–31 607, 2021.
- [5] D. Rupperecht, K. Kohls, T. Holz, and C. Pöpper, "Call me maybe: Eavesdropping encrypted {LTE} calls with {ReVoLTE}," in *29th USENIX security symposium (USENIX security 20)*, 2020, pp. 73–88.
- [6] J. Phillips and M. Mandelkern, "Eavesdropping: What is it good for?" *Semantics and Pragmatics*, vol. 13, pp. 19–1, 2020.
- [7] H. Zhou and A. El Gamal, "Network information theoretic security with omnipresent eavesdropping," *IEEE Transactions on Information Theory*, vol. 67, no. 12, pp. 8280–8299, 2021.
- [8] P. Hu, H. Zhuang, P. S. Santhalingam, R. Spolaor, P. Pathak, G. Zhang, and X. Cheng, "Accear: Accelerometer acoustic eavesdropping with unconstrained vocabulary," in *2022 IEEE Symposium on Security and Privacy (SP)*. IEEE, 2022, pp. 1757–1773.
- [9] Z. Ba, T. Zheng, X. Zhang, Z. Qin, B. Li, X. Liu, and K. Ren, "Learning-based practical smartphone eavesdropping with built-in accelerometer," in *NDSS*, vol. 2020, 2020, pp. 1–18.
- [10] L. Zhang, P. H. Pathak, M. Wu, Y. Zhao, and P. Mohapatra, "Accelword: Energy efficient hotword detection through accelerometer," in *Proceedings of the 13th Annual International Conference on Mobile Systems, Applications, and Services*, 2015, pp. 301–315.
- [11] S. Basak and M. Gowda, "mmspy: Spying phone calls using mmwave radars," in *2022 IEEE Symposium on Security and Privacy (SP)*. IEEE, 2022, pp. 1211–1228.
- [12] A. Kwong, W. Xu, and K. Fu, "Hard drive of hearing: Disks that eavesdrop with a synthesized microphone," in *2019 IEEE symposium on security and privacy (SP)*. IEEE, 2019, pp. 905–919.
- [13] W. Su, D. Liu, T. Zhang, and H. Jiang, "Towards device independent eavesdropping on telephone conversations with built-in accelerometer," *Proceedings of the ACM on Interactive, Mobile, Wearable and Ubiquitous Technologies*, vol. 5, no. 4, pp. 1–29, 2021.
- [14] B. Nassi, Y. Pirutin, R. Swisa, A. Shamir, Y. Elovici, and B. Zadov, "Lamphone: Passive sound recovery from a desk lamp's light bulb vibrations," in *31st USENIX Security Symposium (USENIX Security 22)*, 2022, pp. 4401–4417.
- [15] N. Roy and R. Roy Choudhury, "Listening through a vibration motor," in *Proceedings of the 14th Annual International Conference on Mobile Systems, Applications, and Services*, 2016, pp. 57–69.
- [16] P. Hu, W. Li, R. Spolaor, and X. Cheng, "mmecho: A mmwave-based acoustic eavesdropping method," in *Proceedings of the ACM Turing Award Celebration Conference-China 2023*, 2023, pp. 138–140.
- [17] A. Lilly, "Imsi catchers: hacking mobile communications," *Network Security*, vol. 2017, no. 2, pp. 5–7, 2017.
- [18] B. Hochman, *The listeners: A history of wiretapping in the United States*. Harvard University Press, 2022.
- [19] Y.-F. Zhu, A. Merkel, K. Donda, S. Fan, L. Cao, and B. Assouar, "Nonlocal acoustic metasurface for ultrabroadband sound absorption," *Physical Review B*, vol. 103, no. 6, p. 064102, 2021.
- [20] R. Dong, M. Sun, F. Mo, D. Mao, X. Wang, and Y. Li, "Recent advances in acoustic ventilation barriers," *Journal of Physics D: Applied Physics*, vol. 54, no. 40, p. 403002, 2021.
- [21] Y.-N. Lv, A.-W. Liu, Y. Tan, C.-L. Hu, T.-P. Hua, X.-B. Zou, Y. Sun, C.-L. Zou, G.-C. Guo, S.-M. Hu *et al.*, "Fano-like resonance due to interference with distant transitions," *Physical review Letters*, vol. 129, no. 16, p. 163201, 2022.
- [22] M. B. Lundeberg, Y. Gao, R. Asgari, C. Tan, B. Van Duppen, M. Autore, P. Alonso-González, A. Woessner, K. Watanabe, T. Taniguchi *et al.*, "Tuning quantum nonlocal effects in graphene plasmonics," *Science*, vol. 357, no. 6347, pp. 187–191, 2017.
- [23] H. Kwon, D. Sounas, A. Cordaro, A. Polman, and A. Alù, "Nonlocal metasurfaces for optical signal processing," *Physical review letters*, vol. 121, no. 17, p. 173004, 2018.

- [24] A. Overvig and A. Alù, “Diffractive nonlocal metasurfaces,” *Laser & Photonics Reviews*, vol. 16, no. 8, p. 2100633, 2022.
- [25] A. C. Overvig, S. C. Malek, and N. Yu, “Multifunctional nonlocal metasurfaces,” *Physical Review Letters*, vol. 125, no. 1, p. 017402, 2020.
- [26] Y.-F. Zhu, X.-Y. Zou, B. Liang, and J.-C. Cheng, “Acoustic one-way open tunnel by using metasurface,” *Applied Physics Letters*, vol. 107, no. 11, 2015.
- [27] Y. Ge, H.-x. Sun, S.-q. Yuan, and Y. Lai, “Switchable omnidirectional acoustic insulation through open window structures with ultrathin metasurfaces,” *Physical Review Materials*, vol. 3, no. 6, p. 065203, 2019.
- [28] Y. Zhang, Y. W. Chin, X. Yu, M. Shrestha, G.-K. Lau, B. C. Koo, K. Liu, and Z. Lu, “Ventilated acoustic metasurface with low-frequency sound insulation,” *JASA Express Letters*, vol. 3, no. 7, 2023.
- [29] J. Zhang, W. Rui, C. Ma, Y. Cheng, X. Liu, and J. Christensen, “Remote whispering metamaterial for non-radiative transceiving of ultra-weak sound,” *Nature Communications*, vol. 12, no. 1, p. 3670, 2021.
- [30] Y. Wang, H. Zhao, H. Yang, H. Zhang, T. Li, C. Wang, J. Liu, J. Zhong, D. Yu, and J. Wen, “Acoustically soft and mechanically robust hierarchical metamaterials in water,” *Physical Review Applied*, vol. 20, no. 5, p. 054015, 2023.
- [31] N. Gao, Z. Zhang, J. Deng, X. Guo, B. Cheng, and H. Hou, “Acoustic metamaterials for noise reduction: a review,” *Advanced Materials Technologies*, vol. 7, no. 6, p. 2100698, 2022.
- [32] Y. Cheng, C. Zhou, B. Yuan, D. Wu, Q. Wei, and X. Liu, “Ultra-sparse metasurface for high reflection of low-frequency sound based on artificial mie resonances,” *Nature materials*, vol. 14, no. 10, pp. 1013–1019, 2015.
- [33] G. Wang, Y. Zou, Z. Zhou, K. Wu, and L. M. Ni, “We can hear you with wi-fi!” in *Proceedings of the 20th annual international conference on Mobile computing and networking*, 2014, pp. 593–604.
- [34] T. Wei, S. Wang, A. Zhou, and X. Zhang, “Acoustic eavesdropping through wireless vibrometry,” in *Proceedings of the 21st Annual International Conference on Mobile Computing and Networking*, 2015, pp. 130–141.
- [35] C. Wang, L. Xie, Y. Lin, W. Wang, Y. Chen, Y. Bu, K. Zhang, and S. Lu, “Thru-the-wall eavesdropping on loudspeakers via rfid by capturing sub-mm level vibration,” *Proceedings of the ACM on Interactive, Mobile, Wearable and Ubiquitous Technologies*, vol. 5, no. 4, pp. 1–25, 2021.
- [36] Z. Wang, Z. Chen, A. D. Singh, L. Garcia, J. Luo, and M. B. Srivastava, “Uwhear: Through-wall extraction and separation of audio vibrations using wireless signals,” in *Proceedings of the 18th Conference on Embedded Networked Sensor Systems*, 2020, pp. 1–14.
- [37] C. Xu, Z. Li, H. Zhang, A. S. Rathore, H. Li, C. Song, K. Wang, and W. Xu, “Waveear: Exploring a mmwave-based noise-resistant speech sensing for voice-user interface,” in *Proceedings of the 17th Annual International Conference on Mobile Systems, Applications, and Services*, 2019, pp. 14–26.
- [38] P. Hu, Y. Ma, P. S. Santhalingam, P. H. Pathak, and X. Cheng, “Milliear: Millimeter-wave acoustic eavesdropping with unconstrained vocabulary,” in *IEEE INFOCOM 2022-IEEE Conference on Computer Communications*. IEEE, 2022, pp. 11–20.
- [39] X. Xu, Y. Chen, Z. Ling, L. Lu, J. Luo, and X. Fu, “mmear: Push the limit of cots mmwave eavesdropping on headphones,” in *IEEE INFOCOM 2024-IEEE Conference on Computer Communications*. IEEE, 2024, pp. 351–360.
- [40] J. Han, A. J. Chung, and P. Tague, “Pitchln: eavesdropping via intelligible speech reconstruction using non-acoustic sensor fusion,” in *Proceedings of the 16th ACM/IEEE International Conference on Information Processing in Sensor Networks*, 2017, pp. 181–192.
- [41] S. A. Anand and N. Saxena, “Speechless: Analyzing the threat to speech privacy from smartphone motion sensors,” in *2018 IEEE Symposium on Security and Privacy (SP)*. IEEE, 2018, pp. 1000–1017.
- [42] Y. Michalevsky, D. Boneh, and G. Nakibly, “Gyrophone: Recognizing speech from gyroscope signals,” in *23rd USENIX Security Symposium (USENIX Security 14)*, 2014, pp. 1053–1067.
- [43] H. A. C. Maruri, P. Lopez-Meyer, J. Huang, W. M. Beltman, L. Nachman, and H. Lu, “V-speech: noise-robust speech capturing glasses using vibration sensors,” *Proceedings of the ACM on Interactive, Mobile, Wearable and Ubiquitous Technologies*, vol. 2, no. 4, pp. 1–23, 2018.
- [44] A. T. Mahdad, C. Shi, Z. Ye, T. Zhao, Y. Wang, Y. Chen, and N. Saxena, “Earspy: Spying caller speech and identity through tiny vibrations of smartphone ear speakers,” *arXiv preprint arXiv:2212.12151*, 2022.
- [45] A. Davis, M. Rubinstein, N. Wadhwa, G. J. Mysore, F. Durand, and W. T. Freeman, “The visual microphone: Passive recovery of sound from video,” *ACM Transactions on Graphics*, 2014.
- [46] S. Sami, Y. Dai, S. R. X. Tan, N. Roy, and J. Han, “Spying with your robot vacuum cleaner: eavesdropping via lidar sensors,” in *Proceedings of the 18th Conference on Embedded Networked Sensor Systems*, 2020, pp. 354–367.
- [47] L. Wang, M. Chen, L. Lu, Z. Ba, F. Lin, and K. Ren, “Voicelister: A training-free and universal eavesdropping attack on built-in speakers of mobile devices,” *Proceedings of the ACM on Interactive, Mobile, Wearable and Ubiquitous Technologies*, vol. 7, no. 1, pp. 1–22, 2023.
- [48] F. Ma, Z. Huang, C. Liu, and J. H. Wu, “Acoustic focusing and imaging via phononic crystal and acoustic metamaterials,” *Journal of Applied Physics*, vol. 131, no. 1, 2022.
- [49] R. V. Craster and S. Guenneau, *Acoustic metamaterials: negative refraction, imaging, lensing and cloaking*. Springer Science & Business Media, 2012, vol. 166.
- [50] G. Ji and J. Huber, “Recent progress in acoustic metamaterials and active piezoelectric acoustic metamaterials—a review,” *Applied Materials Today*, vol. 26, p. 101260, 2022.
- [51] J. Ji, C. Zhao, F. Yao, T. Oishi, J. Stewart, and Y. Jing, “Metamaterial-augmented head-mounted audio module,” *Advanced Materials Technologies*, vol. 8, no. 19, p. 2300834, 2023.
- [52] S. Qu, M. Yang, Y. Xu, S. Xiao, and N. X. Fang, “Reverberation time control by acoustic metamaterials in a small room,” *Building and Environment*, vol. 244, p. 110753, 2023.
- [53] W. Zhang, X. Liu, and F. Xin, “Normal incidence sound absorption of an acoustic labyrinthine metal-fibers-based porous metamaterial at high temperature,” *International Journal of Mechanical Sciences*, vol. 237, p. 107821, 2023.
- [54] T. Gu, Z. Wen, L. He, M. Yu, Y. Li, Y. Li, and Y. Jin, “A lightweight metastructure for simultaneous low-frequency broadband sound absorption and vibration isolation,” *The Journal of the Acoustical Society of America*, vol. 153, no. 1, pp. 96–104, 2023.
- [55] V. P. Richmond, “Nonverbal behavior in interpersonal relations,” (*No Title*), p. 366, 2008.
- [56] E. Sundstrom and I. Altman, “Interpersonal relationships and personal space: Research review and theoretical model,” *Human Ecology*, vol. 4, pp. 47–67, 1976.
- [57] M. J. Wieser, P. Pauli, M. Grosseibl, I. Molzow, and A. Mühlberger, “Virtual social interactions in social anxiety—the impact of sex, gaze, and interpersonal distance,” *Cyberpsychology, Behavior, and Social Networking*, vol. 13, no. 5, pp. 547–554, 2010.
- [58] “Sox,” <https://sourceforge.net/projects/sox/>, last accessed: 2024-10-6.
- [59] J. C. Catford, *A practical introduction to phonetics*. Oxford University Press, 2001.
- [60] V. Katinas, M. Marčiukaitis, and M. Tamašauskienė, “Analysis of the wind turbine noise emissions and impact on the environment,” *Renewable and Sustainable Energy Reviews*, vol. 58, pp. 825–831, 2016.
- [61] W. Wang, Y. Yan, Y. Zhao, and Y. Xue, “Studies on the experimental measurement of the low-frequency aerodynamic noise of large wind turbines,” *Energies*, vol. 17, no. 7, p. 1609, 2024.
- [62] O. Heintze, V. Wittstock, and C. F. Hartung, “Sound radiation of a large truck oil pan: Estimation and experimental investigation,” *Journal of the Acoustical Society of America*, vol. 123, no. 5, pp. 3171–3171, 2008.
- [63] B. Zhang, Y. Rao, Y. Guo, and W. Xiao, “Noise reduction performance of metamaterials sound insulation plate,” in *International Conference on Urban Climate, Sustainability and Urban Design*. Springer, 2023, pp. 656–666.
- [64] “Apple,” <https://www.apple.com.cn/iphone/>, last accessed: 2024-10-14.
- [65] “Samsung,” <https://www.samsung.com.cn/smartphones/all-smartphones/>, last accessed: 2024-10-14.
- [66] “Google,” <https://www.google-mobile.cn/>, last accessed: 2024-10-14.
- [67] “Xiaomi,” <https://www.mi.com/>, last accessed: 2024-10-14.
- [68] “Huawei,” <https://consumer.huawei.com/cn/phones/>, last accessed: 2024-10-14.
- [69] J. Kominck, T. Schultz, and A. W. Black, “Synthesizer voice quality of new languages calibrated with mean mel cepstral distortion,” in *SLTU*, 2008, pp. 63–68.
- [70] “Google text-to-speech ai,” <https://cloud.google.com/speech-to-text>, last accessed: 2024-8-6.
- [71] I. Recommendation, “Vocabulary for performance and quality of service,” *International Telecommunications Union—Radiocommunication (ITU-T), RITP: Geneva, Switzerland*, 2006.
- [72] L. Peng, “Sound absorption and insulation functional composites,” in *Advanced high strength natural fibre composites in construction*. Elsevier, 2017, pp. 333–373.
- [73] X. Xu, H. Wang, Y. Sun, J. Han, and R. Huang, “Sound absorbing properties of perforated composite panels of recycled rubber, fiberboard sawdust, and high density polyethylene,” *Journal of Cleaner Production*, vol. 187, pp. 215–221, 2018.